BEDDING GEOMETRY IN THE MEDUSAE FOSSAE FORMATION M. Jodhpurkar[1], R.B. Anderson[2], K. Lewis[3], D. Rubin[4], L. Edgar[2], C. Newman[5]. [1]College of William and Mary, [2]U.S. Geological Survey Astrogeology Science Center (rbanderson@usgs.gov), [3]Johns Hopkins University Applied Physics Laboratory, [4]University of California Santa Cruz, [5]Aeolis Research

Introduction: The Medusae Fossae Formation (MFF) is an expansive deposit of unknown origin located near the equator of Mars, between 170° and 240° E. It is thought to be made of a friable, fine-grained material [1], and the dominant hypotheses for its origin are aeolian, pyroclastic flow, or ash fall deposits [2]. Radar-sounding and gravity data indicate that the MFF has a high porosity and/or low density [1,3]. Many areas of the MFF contain indurated bedforms and extensive yardangs suggesting aeolian reworking and modern bedforms suggesting eventual redeposition [4].

In addition, the MFF has been observed to exhibit "swirling, discontinuous layers" in some locations [4]. These distinctive layers likely indicate non-planar bedding, potentially as a result of cross-bedding. The identification and interpretation of cross-bedding can provide insights into depositional conditions and paleoenvironments. Layering has long been observed in the MFF but this was often interpreted in comparison with the polar layered deposits, and generally used at an inadequate resolution to detect cross-bedding [2,5].

Previously, some authors have noted similarities between the lower member of the MFF and the upper member of Aeolis Mons, in Gale crater. Curvilinear bedding patterns have been observed in upper Aeolis Mons [6], and bedding geometry measurements indicate an aeolian origin [7]. Both areas also display regular bedding patterns in some locations, with a bedding scale of 4.5 m in the upper Gale mound and 2.8-3.4 m in the MFF [8,9]. If these deposits are related [10], it would be consistent with the hypothesis that the MFF was once significantly more extensive [11].

In this study, we measured the geometry of some apparent non-planar beds in the MFF. These measurements can constrain the processes involved in MFF deposition, and be compared with similar measurements in upper Aeolis Mons in Gale crater.

Samples and Methods: Two HiRISE image stereo pairs were used for this study; PSP_006616_1730/ ESP_024285_1730 (mff1) and ESP_046887_1695/ ESP_046742_1695 (mff2), located in the center and on the edge of Lucus Planum (the central part of the MFF), respectively. These sites were selected because they appeared to exhibit complex bedding geometry. We used ArcGIS to trace most of the recognizable beds in the image, allowing us to visualize bedding patterns and the broad trends across the image (Fig. 1).

In MatLab, we extracted topographic profiles along the edge of beds and found the best fit plane to the selected points. This procedure can be strongly biased by

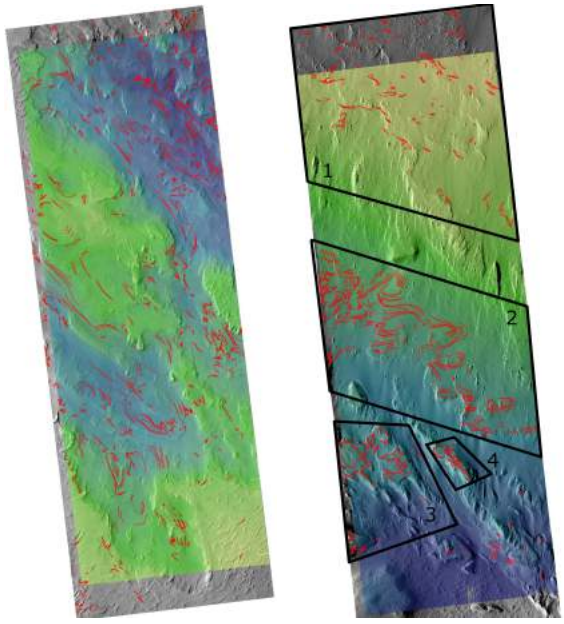

Figure 1: DTM of mff1 (left) and mff2 (right), with high elevations depicted in yellow. Beds traced in ArcGIS are shown in red. Black polygons show distinct areas in the image, identified through analysis of bedding patterns.

plane fits that conform to the local surface rather than the angled bedding that intersects the surface, so we implement a series of strict tests to ensure the quality of the measurements. Measurements for which the angular uncertainty was greater than 1° were considered poorly constrained and rejected. When a bed trace did not achieve an acceptable fit after tracing for 250 m, the trace was rejected, resulting in curved beds being split into several local plane fits rather than a single overall fit. If the angular difference between the orientation of the local patch of topography and that of the bed trace best-fit plane was smaller than a threshold value, that measurement was excluded as being too similar to the local surface orientation to ensure that we were tracing beds in outcrop, not surfaces. Every best-fit plane was visualized as it intersected with topography. Areas where the plane's intersection was irregular and did not follow the bed trace and surrounding beds were excluded from analysis. Cases where the orientation of one measurement contradicted other measurements from the same set of beds were also removed.

Once all the measurements were checked for accuracy, we visualized the dip azimuths and magnitudes (Fig. 2). This led us to split the image into four areas, where topographic or other boundaries separated areas of bedding from each other. Rose diagrams (Fig. 3) of

these areas were also created and compared to simulations [12] to aid in interpretation of bedding patterns.

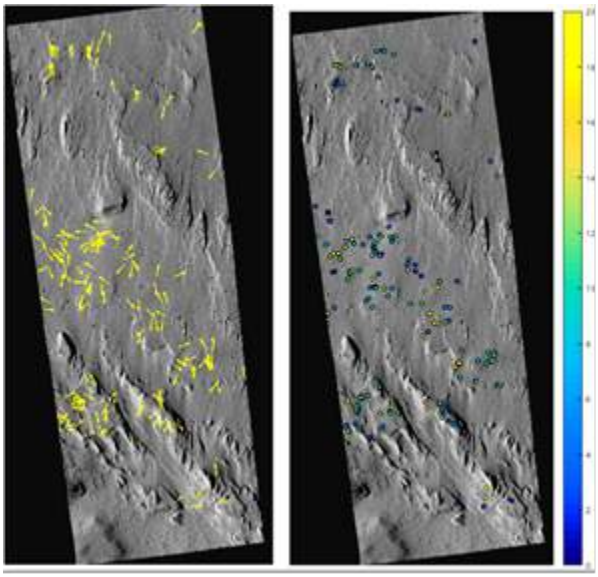

Figure 2: Dip azimuths (left) depicted by yellow arrows and dip magnitudes (right) represented by colored dots.

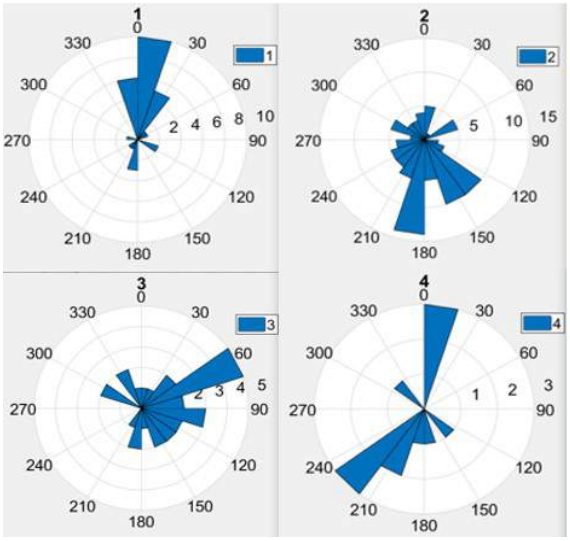

Figure 3: Rose diagrams of dip azimuth for the four areas in mff2 (Fig. 1).

Results and Discussion: From the 1078 measurements conducted on mff2, 174 were determined to be "good" after the rigorous quality checks described above. These measurements exhibited a general north-south trend in dip azimuths, but local trends towards other directions that suggested the measurements needed to be grouped into four smaller areas (Fig. 3). Within this DTM, the appearance of exposed bedding often varied. It was very well expressed in some areas and almost indiscernible in others. The dip magnitudes tended to be shallow, with most ranging from 1 to 14°.

Area 1 contains sparse, faint bedding. The dips generally point north, in the opposite direction of the regional slope. Area 2 displays convoluted bedding patterns, including several concentric bedding features, in an area with little elevation change. This indicates that topography has little influence and that the patterns are primarily due to non-planar bedding geometry. The dips in Area 2 trend toward the south with a weakly bimodal distribution. Area 3 is located on a topographic high, and while some of the complex bedding is influenced by the topography, there were many deviations. Here, most dips trended towards the east. Area 4 is the smallest area identified, but it was separated from Area 3 as it is a separate ridge and had a very different rose plot. This area had two broad trends, with dips pointing north and southwest.

Shallow dip magnitudes are potentially consistent with the pyroclastic or aeolian hypothesis. However, the rose plots for Areas 2 and 4 match simulations of superimposed bedforms [12], consistent with an aeolian dune field origin. Based on these observations, it seems likely that the curvilinear patterns observed in this part of the MFF resulted from aeolian cross-beds. The rhythmic nature of the bedding, along with its swirling patterns, are harder to explain with a pyroclastic flow origin. The variation in the rose plots suggests changes in the bedform style and flow direction which is difficult to explain with pyroclastic flow deposits.

Future Work: Future work involves checking the planes for the 1024 measurements gathered for mff1 and analyzing the dip azimuths and magnitudes there in comparison with those from mff2. We will also generate custom bedform simulations for both sites to aid in interpretation of the bedding geometry. The measurements will be compared to those taken at Aeolis Mons to identify any similarities. Additionally, future mesoscale atmospheric modeling efforts can be used to compare modern prevailing wind azimuths with those inferred from cross bedding.

Acknowledgements: This material is based on work supported by the NASA MDAP Grant No. NNH14AY24I and the NSF Grant No. AST-1461200.

References: [1] Carter, L.M. et al. (2009) *Icarus*, 199, 295–302. [2] Mandt, K.E. et al. (2009) *J. Geophys. Res.,* 113, E12011. [3] Ojha et al. (2017) LPS XLVIII, 2475l. [4] Kerber, L., Head, J.W. (2012) Earth *Surf. Process. Landf.,* 37, 422–433. [5] Bradley, B.A. et al. (2002) *J. Geophys. Res.,* 107, E8, 2.1–2.17. [6] Anderson, R.B., Bell, J.F. (2010) *Mars J.* 5, 76–128. [7] Anderson, R.B. et al. (2018) *Icarus*, In Review. [8] Lewis, K.W., Aharonson, O. (2014) *J. Geophys. Res. Planets* 119, 1432–1457. [9] Zimbelman, J.R., and Scheidt, S.P. (2012) *Science*, 336, 6089, 1683. [10] Thomson, B.J. et al., (2011) *Icarus,* 214, 413–432. [11] Schultz, P.H. and Lutz, A.B. (1988) *Icarus,* 73, 91–141 [12] Rubin, D.M. and Carter, C.L. (2006*) Concepts in Sedimentology and Paleontology.*